Signals of 660-km topography and harzburgite enrichment in seismic images of whole-mantle upwellings

Ross Maguire[1], Jeroen Ritsema[1], Saskia Goes[2]

[1]Department of Earth and Environmental Sciences, University of Michigan, Ann Arbor, MI, 48109-1005, USA
[2]Department of Earth Science and Engineering, Imperial College London, London, SW7 2AZ, United Kingdom

Key Points:

- A narrow high seismic velocity anomaly near the 660-km phase boundary splits a mantle-wide low seismic velocity anomaly beneath Samoa.
- Harzburgite enrichment below the base of transition zone within a continuous hot thermochemical upwelling can explain the 'Samoa gap'.
- Anomaly strength can be matched by a harzburgite fraction of at least 0.925 and a temperature elevated by 125–175°C.

Corresponding author: Ross Maguire, romaguir@umich.edu

Abstract

Various changes in seismic structures across the mantle transition zone (MTZ) indicate it may hamper thermal and chemical circulation. Here we show how thermal elevation of the post-spinel phase transition at 660 km depth plus harzburgite segregation below this depth can project as narrow high-velocity anomalies in tomographic images of continuous thermochemical mantle upwellings. Model S40RTS features a narrow high-velocity anomaly of +0.8% near 660 km depth within the broad low-velocity structure beneath the Samoa hotspot. Our analyses indicate that elevation of the 660 phase boundary in a hot pyrolitic plume alone is insufficient to explain this anomaly. An additional effect of harzburgite enrichment is required and consistent with geodynamic simulations that predict compositional segregation in the MTZ, especially within thermochemical upwellings. The Samoa anomaly can be modelled with a 125–175°C excess temperature and a harzburgite enrichment below 660 of least 60% compared to a pyrolitic mantle.

1 Introduction

It is well established that the upper mantle transition zone has a profound influence on the structure of mantle flow. Seismic tomography has been successful in imaging the variable descent of subducting slabs into the deep mantle [e.g., *Grand*, 1994; *Sigloch and Mihalynuk*, 2013; *Fukao and Obayashi*, 2013] but tomographic constraints on the origin of mantle upwellings have remained ambiguous [e.g., *Montelli et al.*, 2004; *Wolfe et al.*, 2009; *Styles et al.*, 2011; *French and Romanowicz*, 2015].

In this paper, we investigate the effects of compositional layering in the upper mantle transition zone on images of mantle upwellings. We consider a thermochemical upwelling from the lower mantle that has transported compositionally distinct material into the transition zone [e.g., *Xie and Tackley*, 2004; *Brandenburg and van Keken*, 2007; *Nakagawa et al.*, 2010]. The layering originates from thermal perturbations of the 660-km phase boundary (i.e., the 660) and from the segregation of basaltic and harzburgitic components with intrinsically different densities [*Irifune and Ringwood*, 1993]. Using a forward modeling approach, we illustrate how anomalous layering near the 660 can project as a high-velocity seismic anomaly embedded within a whole-mantle low-velocity structure and be reminiscent of discontinuous flow across the transition zone.

Figure 1a is the working example of our analysis. It shows the shear-velocity structure in the mantle beneath the southwestern Pacific according to S40RTS [*Ritsema et al.*, 2011]. The dipping high-velocity anomaly between 10^o and 35^o is the subducting Pacific Plate. A broad low-velocity anomaly extends from the core-mantle boundary to the surface beneath the Samoa hotspot. We interpret this mantle-wide structure as a large-scale mantle upwelling related to hotspot volcanism on Samoa and call it the *Samoa plume* for simplicity. There is a gap in the Samoa plume near the base of the upper-mantle transition zone, manifested as a positive wave speed anomaly with a maximum amplitude of δV_S = 0.8%. We will call this the *Samoa gap* from here on. The Samoa gap may imply that upward mantle flow is blocked near the 660. Here, we hypothesize that the Samoa gap is due to the thermal elevation of the 660 and compositional heterogeneity around the base of the transition zone within a continuous thermochemical upwelling. Our modeling is informed by seismic estimates of 660 topography, geodynamic simulations of mantle mixing, and estimates of image resolution in tomographic model S40RTS.

2 Models of the Samoa gap

2.1 Temperature induced phase boundary topography

The mineral phase transformation of ringwoodite (ri) to the post–spinel phases bridgemanite (br) plus magnesiowüstite (mw) is responsible for the deepest global seismic discontinuity in the upper mantle at 660 km depth. Recent estimates indicate that this transition has a negative Clapeyron slope $-2.9 \leq \gamma_{660} \leq -2.1$ MPa K^{-1} [*Ye et al.*, 2014]. Hence, a temperature increase in the upper mantle of $\Delta T = 250°$C would elevate the 660 by 13–18 km. Analyses of P and S wave reflections [e.g., *Flanagan and Shearer*, 1998; *Gu and Dziewonski*, 2002; *Deuss*, 2009] and conversions [e.g., *Schmandt et al.*, 2012; *Mulibo and Nyblade*, 2013; *Jenkins et al.*, 2016] indicate that topography on the 660 in the mantle is as high as 30 km.

In seismic images (Figure 1b), a locally elevated 660 would be visible as a thin high-velocity anomaly with respect to a mantle in which the 660 is unperturbed. Its vertical width is equivalent to the elevation of the 660 and the velocity contrast is determined by the shear velocity increase across the 660. The expected concurrent depression of the 410 due to the exothermic phase transition around that depth would produce a low-velocity anomaly. We ignore such an anomaly because it would likely not be observable within a large-scale low-velocity anomaly (i.e., the Samoa plume).

2.2 Basalt depletion below the 660

Melting of mantle peridotite generates a stratified oceanic lithosphere with layers of basalt and harzburgite. After plates subduct these two components are recycled back into the mantle to become a folded and stretched mechanical mixture (see *Xu et al.* [2008] for a discussion). Since harzburgite is denser than mid-ocean ridge basalt for a narrow depth range ($\sim$ 100 km) beneath the 660, the two components may segregate near the 660 [*Irifune and Ringwood*, 1993]. As a result the lower mantle will have a harzburgite enriched composition between about 660 and 800 km depth and basalt enrichment directly above 660. Numerical simulations of thermochemical mantle convection [e.g., *Xie and Tackley*, 2004; *Brandenburg and van Keken*, 2007; *Nakagawa et al.*, 2010] demonstrate that a compositional gradient forms in the mantle and that basalt–harzburgite partitioning can be particularly strong within upwelling regions of the mantle and when γ_{660} or the density contrast between basalt and harzburgite are high [e.g., *van Summeren et al.*, 2009]. The shear velocity of a basalt-enriched composition above 660 will be lower than the background mantle and would contribute to the overall low velocities of a hot upwelling. By contrast, the shear speed in a harzburgite-enriched layer beneath the 660 is higher than in a mantle with a pyrolite composition, as illustrated in Figure 1c.

3 Analysis

3.1 Mineral physics constraints

Experimental mineral physics results constrain our seismic models of the elevation of the 660 and harzburgite enrichment in the uppermost lower mantle. We compute theoretical profiles of shear velocity as described in *Cobden et al.* [2008], i.e., using PerPle_X [*Connolly*, 2005], with the thermodynamic parameter database from *Stixrude and Lithgow-Bertelloni* [2011] and estimates of temperature and pressure-dependent anelasticity from *Goes et al.* [2004]. As in *Xu et al.* [2008], the mantle is composed of the Na-Ca-Fe-Mg-Al-Fi (i.e, NCFMAS) oxides and regarded as a mechanical mixture of basalt and harzburgite in proportions f and 1–f, respectively. We calculate the reference profile for an adiabat with a potential temperature of 1300°C, suitable for the convective MORB-source mantle, and for a basalt fraction $f = 0.2$, roughly equivalent to the composition of pyrolite. We compute the elevation of the 660 due to a temperature increase using a Clapeyron slope of $\gamma_{660} = -2.9$ MPa K^{-1} and velocity anomalies due to changes in the composition of the uppermost lower mantle by changing f.

Figure 2a compares profiles of shear velocity for basalt fractions f between 0 and 0.4 and an adiabat for the reference potential temperature of 1300°C. In a purely harzburgitic mantle (i.e., $f = 0$), the 660 phase transition is entirely controlled by the $ri \rightarrow bm + mw$ transition with a shear velocity jump of 9.0% at the 660. The shear velocity is up to 2% higher than in a pyrolitic mantle between 660 km and 760 km depth. In a mechanical mixture of basalt and harzburgite (i.e., $f > 0$), the phase transformation at the 660 is distributed over a finite pressure range because the $gt \rightarrow mw$ in basalt occurs near 760 km depth. The shear velocity jump at the 660 decreases with increasing basalt fraction f from 7.2% for $f = 0.2$ to 5.4% for $f = 0.4$. Figure 2b compares profiles of shear velocity for adiabats with potential temperatures between 1300°C (our reference geotherm) and 1600°C (expected within a hot mantle upwelling). The basalt fraction f = 0.2. The elevation of the 660 increases with temperature but the velocity increase across the 660 is not very sensitive to temperature.

3.2 Model parameterization

We parameterize the elevation of the 660 and a layer below the 660 with a harzburgite-enriched composition as narrow rectangular blocks. The rectangular blocks have horizontal side lengths of 1000 km which corresponds to the minimum horizontal scale that can be resolved by S40RTS. The vertical thickness H and the uniform velocity perturbation $\delta \mathrm{V_{IN}}$ are free parameters.

For a model that represents a 660 perturbation, H corresponds to the elevation of the 660. The shear velocity jump $\delta \mathrm{V_B}$ at the phase boundary (see Figure 2c) and the shear velocity reduction $\delta \mathrm{V_T}$ due to the increased temperature determine $\delta \mathrm{V_{IN}}$ (see Figure 2d). $\delta \mathrm{V_{IN}} = \delta \mathrm{V_B} + \delta \mathrm{V_T}$. For a model that represents a harzburgite-enriched layer beneath the 660, H is the layer thickness and the shear velocity anomaly $\delta \mathrm{V_{IN}}$ depends on the composition (δV_{C}) and temperature $\delta \mathrm{V_T}$. Thus, $\delta \mathrm{V_{IN}} = \delta \mathrm{V_C} + \delta \mathrm{V_T}$, where $\delta \mathrm{V_C}$ and $\delta \mathrm{V_T}$ have opposite signs. If the layer is pure harzburgite ($f = 0$) and there is no temperature anomaly, then $\delta \mathrm{V_{IN}}$ is about 2%. If ΔT exceeds about 200°C, the shear velocity in the harzburgite-enriched layer is lower than in the reference model and the layer may not be visible.

3.3 Tomographic filtering

To estimate how phase boundary topography and harzburgite enrichment in the uppermost lower mantle would be imaged tomographically, we use the model resolution matrix $\mathcal{R}$

of S40RTS. We first project the test structure (i.e., the rectangular block) into the model parameterization of S40RTS, which consists of spherical harmonics up to degree 40, and 21 vertical spline basis functions. After projection into S40RTS parameterization the linear operator $\mathcal{R}$ is applied to produce a tomographically filtered version of the input model. Application of $\mathcal{R}$ distorts and dampens the input model due to incomplete and heterogeneous data coverage, and model regularization, but it does not include the effects of inaccurate forward modeling [*Ritsema et al.*, 2007].

Figure 3 shows how a 30-km elevation of the 660 (in Figure 3a) and a 100-km thick layer of compositional heterogeneity below the 660 (in Figure 3b) would be imaged in S40RTS. After projection into S40RTS parameterization (Figure 3c and 3d) the high-velocity rectangular blocks are thicker and the velocity anomalies are weaker because the spacing of the vertical splines in S40RTS is large compared to H. The amplitude reduction is strongest for the thinnest layer. After filtering (Figure 3e and 3f), the velocity perturbations have been reduced further by a factor of about two.

4 Results

The contours in Figure 4 show how the peak recovered velocity anomaly, which we refer to as $\delta\mathrm{V_{OUT}}$, varies as function of H and $\delta\mathrm{V_{IN}}$. $\delta\mathrm{V_{OUT}}$ depends linearly on $\delta\mathrm{V_{IN}}$ and non-linearly on H. It is highest for the thickest layers when re-parameterization affects the amplitude reduction the least.

In Figure 4a, the highest value for $\delta\mathrm{V_{OUT}}$ of 1.7% is obtained when the 660 is elevated by 30 km and the shear velocity jump across the 660 is 10%. The Samoa gap of 0.8% (see Figure 1) can be explained if the 660 is elevated by at least 15 km. For a shear velocity jump as small as 5%, the 660 elevation must be 25 km or more. The smallest shear velocity perturbation $\delta\mathrm{V_{IN}}$ in combination with the smallest H for which $\delta\mathrm{V_{OUT}} = 0.8\%$ are 7% and 18 km, respectively. The combinations of H and $\delta\mathrm{V_{IN}}$ consistent with a temperature induced elevation of the 660, as discussed in Section 3.1, are indicated by dashed lines in Figure 4a. We consider a mantle mixture with a pyrolitic composition ($f = 0.2$) and a harzburgitic mantle ($f = 0$) and assume that γ_{660} = -2.9 MPa K^{-1}. The highest values of $\delta\mathrm{V_{OUT}}$ are obtained when ΔT is about 200–250°C, depending on composition. Within this temperature range, the 660 elevation is about 15–20 km. $\delta\mathrm{V_{OUT}}$ approaches 0.8% if the mantle is composed of pure harzburgite but it is smaller than 0.5% for a pyrolitic mantle.

Figure 4b shows that the Samoa gap of 0.8% can be better explained by a harzburgite-enriched layer with a thickness of at least 50 km. The highest value for $\delta \mathrm{V_{OUT}}$ of 1.7% is obtained when shear velocity jump is 2.1% higher than in the ambient mantle within 100-km thick layer below the 660. The smallest values for $\delta \mathrm{V_{IN}}$ and H for which $\delta \mathrm{V_{OUT}} = 0.8\%$ are 1.5% and 70 km, respectively. The shear velocity increase $\delta \mathrm{V_{IN}}$ in this layer decreases with increasing basalt fraction f. If the layer has a thickness of 100 km, the harzburgite fraction must be higher than 0.925 to match the Samoa gap of 0.8%.

5 Discussion and Conclusions

In this paper, we have demonstrated that thermal elevations of the post-spinel phase transition at 660 km depth and basalt segregation at the top of the lower mantle can project as narrow high-velocity anomalies in tomographic images of continuous thermochemical mantle upwellings. Even though our analysis used post–spinel Clapeyron slopes on the high end of those determined from mineral physics [*Ye et al.*, 2014; *Hirose*, 2002; *Weidner and Wang*, 1998], the elevation of the 660 alone is not sufficient to explain the relatively high shear velocity in the Samoa gap. This is because of the competing effects of the phase transition and temperature on shear velocity in a pyrolytic mantle. A harzburgite-enriched layer within the uppermost lower mantle is an essential feature of the model. It is consistent with geodynamic simulations of mantle mixing which predict strong compositional layering around the 660 [e.g., *Xie and Tackley*, 2004; *Nakagawa et al.*, 2010; *van Summeren et al.*, 2009]. It may also help explain the change in the pattern of seismic velocity heterogeneity across the 660 [e.g., *Gu et al.*, 2001; *Ritsema et al.*, 2004].

In Figure 5 we show which combinations of mantle temperature anomaly ΔT and composition below 660 can explain the high velocity anomaly of 0.8% in the gap within the thermochemical Samoa plume (See Figure 1). The uppermost lower mantle is enriched in harzburgite due to compositional segregation across the 660. Assuming a Clapeyron slope for the 660 phase boundary of γ_{660} = -2.9 MPa K^{-1}, we find that if the average harzburgite fraction is $>$ 0.925 (i.e., a basalt fraction of f $<$ 0.075) between 660 and 760 km depth, a temperature anomaly of ΔT = 125–175°C in the transition zone can explain the Samoa anomaly. Although phase boundary topography plus high-velocity material below or around 660 km depth are required to match the Samoa gap, estimates of composition and thermal anomaly are subject to substantial uncertainties associated with the mineral physics constraints on transition-zone shear velocities [*Stixrude and Lithgow-Bertelloni*, 2011; *Cammarano et al.*, 2003].

Our analysis has focused on the mantle beneath the Samoa hotspot where image resolution in the transition zone is relatively high and where the effects are most obvious. The Samoa plume and gap are also apparent in tomographic models based on different data sets and modeling strategies (Supplementary Figure 1). However, a quantitative comparison of image resolution for all models is necessary to determine whether these tomographic images are consistent with S40RTS and our analysis.

While this study has concentrated on anomalies caused by phase boundary effects in regions of mantle upwelling, we expect that within a cold slab the $ri \rightarrow bm + mw$ transition will occur at a greater depth, and thus introduce a thin low wavespeed anomaly. The Pacific slab anomaly (Figure 1a) is diminished by about 0.5% near 660, which is consistent with this interpretation. Figure 4a indicates that if the average slab composition is close to pyrolite, a velocity anomaly of 0.5% can be explained by a thermally induced phase boundary deflection of 15 km, corresponding to a temperature decrease within the slab of $\Delta \mathrm{T} = 200^\circ$ C.

If harzburgite-enrichment is important in the mantle, we should expect to see high-velocity anomalies in other regions of mantle upwelling. Anomalies similar to the gap in the Samoa plume are indeed apparent beneath the Azores, Canary, Galapagos, and Hawaii hotspots (Supplementary Figure 2) although they are much weaker and not as obviously layered, most likely due to the relatively poor tomographic image resolution in the transition zone beneath regions far from the western Pacific subduction zones [e.g., *Ritsema et al.*, 2004; *Houser et al.*, 2008] (Supplementary Figure 3).

While we suggest that high-velocity layering within broad low seismic velocity anomalies is consistent with dynamically predicted basalt–harzburgite segregation, this prediction depends on the post-spinel Clapeyron slope [*Weinstein*, 1992], mantle viscosity [*Brandenburg and van Keken*, 2007] and the relative densities of basalt, harzburgite and pyrolite as a function of pressure and temperature, each with significant uncertainties. These parameters determine whether or not global compositional stratification near 660 develops over the convective timescale of Earth [*Nakagawa et al.*, 2010]. Further work should test our observation and interpretation of the compositional segregation within mantle plumes.

Acknowledgments

This work has been funded by NSF grant EAR–1565511 to JR and by NERC grant NE/J008028/1 to SG. We acknowledge computational support from XSEDE and travel support via a Turner fund from the University of Michigan. We also thank Scott King and an anonymous reviewer for helpful comments which improved this paper. All data necessary to reproduce our analysis is included in the supplemental material.

References

Brandenburg, J. P., and P. E. van Keken (2007), Deep storage of oceanic crust in a vigorously convecting mantle, *J. Geophys. Res.: Solid Earth*, *112*(6), 1–15, doi: 10.1029/2006JB004813.

Cobden, L., S. Goes, F. Cammarano, and J. A. D. Connolly (2008), Thermochemical interpretation of one-dimensional seismic reference models for the upper mantle: Evidence for bias due to heterogeneity, *Geophys. J. Int.*, *175*(2), 627–648, doi: 10.1111/j.1365-246X.2008.03903.x.

Cammarano, F., S. Goes, P. Vacher, and D. Giardini (2003). Inferring upper-mantle temperatures from seismic velocities, *Phys. Earth Planet. Inter.*, 138(3–4), 197–222. doi: http://doi.org/10.1016/S0031-9201(03)00156-0

Connolly, J. A. D. (2005), Computation of phase equilibria by linear programming: A tool for geodynamic modeling and its application to subduction zone decarbonation, *Earth Planet. Sci. Lett.*, *236*(1-2), 524–541, doi:10.1016/j.epsl.2005.04.033.

Deuss, A. (2009), Global observations of mantle discontinuities using SS and PP precursors, *Surveys in Geophysics*, *30*(4-5), 301–326, doi:10.1007/s10712-009-9078-y.

Flanagan, M. P., and P. M. Shearer, (1998), Global mapping of topography on transition zone velocity discontinuities by stacking SS precursors, *J. Geophys. Res.: Solid Earth*, *103*(B2), 2673–2692.

French, S. W., and B. Romanowicz(2015), Broad plumes rooted at the base of the Earth's mantle beneath major hotspots, *Nature*, *525*(7567), 95–99, doi:10.1038/nature14876.

Fukao, Y., and M. Obayashi (2013), Subducted slabs stagnant above, penetrating through, and trapped below the 660 km discontinuity, *Journal of Geophysical Research: Solid Earth*, *118*(11), 5920–5938, doi:10.1002/2013JB010466.

Goes, S., F. Cammarano, and U. Hansen (2004), Synthetic seismic signature of thermal mantle plumes, *Earth Planet. Sci. Lett.*, *218*(3-4), 403–419, doi:10.1016/S0012-821X(03)00680-0.

Grand, S. P. (1994), Mantle shear structure beneath the Americas and surrounding oceans, *J. Geophys. Res.*, *99*(B6), 11,591, doi:10.1029/94JB00042.

Gu, Y. J., A.. M. Dziewonski, W.-J. Su, and G. Ekström (2001), Models of the mantle shear velocity and discontinuities in the pattern of lateral heterogeneities, *J. Geophys. Res.* , *106* ,11169-11199

Gu, Y. J., and A. M. Dziewonski (2002), Global variability of transition zone thickness, *J. Geophys. Res*, *107*(B7), 2135, doi:10.1029/2001JB000489.

Hirose, K. (2002), Phase transitions in pyrolitic mantle around 670-km depth: Implications for upwelling of plumes from the lower mantle, *J. Geophys. Res.: Solid Earth*, *107*(B4), ECV 3–1–ECV 3–13, doi:10.1029/2001JB000597.

Houser, C., G. Masters, P. M. Shearer, and G. Laske, (2008). Shear and compressional velocity models of the mantle from cluster analysis of long-period waveforms *Geophys. J. Int.*, *174*(1), 195–212, doi:10.1111/j.1365-246X.2008.03763.x.

Irifune, T., and A. E., Ringwood (1993), Phase transformations in subducted oceanic crust and buoyancy relationships at depths of 600-800 km in the mantle, *Earth Planet. Sci. Lett.*, *117*(1-2), 101–110, doi:10.1016/0012-821X(93)90120-X.

Jenkins, J., S. Cottaar, R. S. White, and A. Deuss (2016), Depressed mantle discontinuities beneath Iceland: Evidence of a garnet controlled 660 km discontinuity?, *Earth Planet. Sci. Lett.*, *433*, 159–168, doi:10.1016/j.epsl.2015.10.053.

Montelli, R., G. Nolet, F. A. Dahlen, G. Masters, E. R. Engdahl, and S. H. Hung (2004), Finite-frequency tomography reveals a variety of plumes in the mantle., *Science*, *303*(5656), 338–343, doi:10.1126/science.1092485.

Mulibo, G. D., and A. A. Nyblade (2013), Mantle transition zone thinning beneath eastern Africa: Evidence for a whole-mantle superplume structure, *Geophys. Res. Lett.*, *40*(14), 3562–3566, doi:10.1002/grl.50694.

Nakagawa, T., P. J. Tackley, F. Deschamps, and J. A. D. Connolly (2010), The influence of MORB and harzburgite composition on thermo-chemical mantle convection in a 3-D spherical shell with self-consistently calculated mineral physics, *Earth Planet. Sci. Lett.*, *296*(3-4), 403–412, doi:10.1016/j.epsl.2010.05.026.

Ritsema, J., H. J. Van Heijst, and J. H. Woodhouse, (2004), Global transition zone tomography, *J. Geophys. Res.*, *109*(B2), B02,302, doi:10.1029/2003JB002610.

Ritsema, J., A. K. McNamara, and A. L.Bull (2007), Tomographic filtering of geodynamic models: Implications for models interpretation and large-scale mantle structure, *J. Geophys. Res.: Solid Earth*, *112*(1), 1–8, doi:10.1029/2006JB004566.

Ritsema, J., A. Deuss, H. J. Van Heijst, and J. H. Woodhouse (2011), S40RTS: A degree-40 shear-velocity model for the mantle from new Rayleigh wave dispersion, teleseismic traveltime and normal-mode splitting function measurements, *Geophys. J. Int.*, *184*(3), 1223–1236, doi:10.1111/j.1365-246X.2010.04884.x.

Schmandt, B., K. G. Dueker, E. D. Humphreys, and S. Hansen (2012), Hot mantle upwelling across the 660 beneath Yellowstone, *Earth Planet. Sci. Lett.*, *331-332*, 224–236, doi:10.1016/j.epsl.2012.03.025.

Sigloch, K., and M. G. Mihalynuk (2013), Intra-oceanic subduction shaped the assembly of Cordilleran North America, *Nature*, *496*(7443), 50–56, doi:10.1038/nature12019.

Stixrude, L., and C. Lithgow-Bertelloni (2011), Thermodynamics of mantle minerals - II. Phase equilibria, *Geophys. J. Int.*, *184*(3), 1180–1213, doi:10.1111/j.1365-246X.2010.04890.x.

Styles, E. E., S. Goes, P. E. van Keken, J. Ritsema, and H. E. Smith (2011), Synthetic images of dynamically predicted plumes and comparison with a global tomographic model, *Earth Planet. Sci. Lett.*, *311*(3-4), 351–363, doi:10.1016/j.epsl.2011.09.012.

van Summeren, J. R. G., A. P. van den Berg, and R. D. van der Hilst (2009), Upwellings from a deep mantle reservoir filtered at the 660 km phase transition in thermo-chemical convection models and implications for intra-plate volcanism, *Phys. Earth Planet. Inter.*, *172*(3-4), 210–224, doi:10.1016/j.pepi.2008.09.011.

Weidner, D. J., and Y. Wang (1998), Chemical-and clapeyron-induced buoyancy at the 660 km discontinuity, *J. Geophys. Res.: Solid Earth*, *103*(B4), 7431–7441.

Weinstein, A. S., (1992) Induced compositional layering in a convecting fluid layer by an endothermic phase transition *Earth Planet. Sci. Lett.* *113*, 23–29 doi:10.1016/0012-821X(92)90209-E

Wolfe, C. J., S. C. Solomon, G. Laske, J. a. Collins, R. S. Detrick, J. a. Orcutt, D. Bercovici, and E. H. Hauri (2009), Mantle shear-wave velocity structure beneath the Hawaiian hot spot., *Science*, *326*(5958), 1388–1390, doi:10.1126/science.1180165.

Xie, S., and P. J. Tackley (2004), Evolution of helium and argon isotopes in a convecting mantle, *Phys. Earth Planet. Inter.*, *146*(3-4), 417–439, doi:10.1016/j.pepi.2004.04.003.

Xu, W., C. Lithgow-Bertelloni, L. Stixrude, and J. Ritsema (2008), The effect of bulk composition and temperature on mantle seismic structure, *Earth Planet. Sci. Lett.*, *275*(1-2), 70–79, doi:10.1016/j.epsl.2008.08.012.

Ye, Y., C. Gu, S.-h. Shim, Y. Meng, and V. Prakapenka (2014), The postspinel boundary in pyrolitic compositions determined in the laser-heated diamond anvil cell, *Geophys. Res. Lett.*, pp. 3833–3841, doi:10.1002/2014GL060060.1.

Figure1.pdf

Figure 1. (a) Vertical, SW–NE oriented cross-section through the shear velocity model S40RTS [*Ritsema et al.*, 2011] centered on the Samoa hotspot. The Samoa plume is a broad low shear velocity anomaly from the core-mantle boundary to the surface and assumed to be a hot thermal upwelling. A high-velocity anomaly breaks the Samoa plume near the 660-km discontinuity (dashed line). This feature is called the Samoa gap in this paper. (b) Sketch of the expected 660-km phase boundary elevation due to the increased temperature in the upper mantle beneath Samoa. (c) Sketch of a layer in the uppermost lower mantle with a harzburgite-enriched composition. The 660 elevation (in b) and the harzburgite-enriched layer (in c) may be observed as high-velocity anomalies.

Figure2.pdf

Figure 2. Shear velocity profiles calculated for mechanical mixtures of basalt and harzburgite in proportions f and $1{-}f$, respectively. (a) The basalt fraction f is varied from 0 to 0.4. The geotherm is an adiabat with a potential temperature of 1300°C. (b) The potential temperature is varied between 1300°C and 1600°C. The basalt fraction $f = 0.2$. (c) The shear velocity increase $\delta\mathrm{V_B}$ across the 660 as a function of basalt fraction f. (d) The shear velocity decrease $\delta\mathrm{V_T}$ in the uppermost lower mantle as a function of temperature increase $\Delta\mathrm{T}$.

Figure3.pdf

Figure 3. Resolution test showing how a rectangular block-shaped velocity anomaly above the 660 (in a) and below the 660 (in b) would be imaged in S40RTS. The anomaly has horizontal side lengths of 1000 km. In (a) the thickness $H = 30$ km and $\delta \mathrm{V}_{\mathrm{IN}} = 5\%$. In (b) the thickness $H = 100$ km and $\delta \mathrm{V}_{\mathrm{IN}} = 2\%$. The anomalies are drawn with vertical exaggeration for clarity. Panels (c) and (d) show these anomalies after projection into S40RTS parameterization. Panels (e) and (f) show the anomalies after re-parameterization and filtering by $\mathcal{R}$. The highest recovered anomaly in tomographically filtered model is $\delta \mathrm{V}_{\mathrm{OUT}}$.

Figure4.pdf

Figure 4. Contours of the peak recovered velocity anomaly $\delta\mathrm{V}_{\mathrm{OUT}}$ obtained by tomographic filtering of input models using $\mathcal{R}$. An input model is defined by the assumed layer thickness H (along the x-axis) and velocity anomaly $\delta\mathrm{V}_{\mathrm{IN}}$ (along the y-axis) and represents (in a) an elevation of the 660 or (in b) a layer in the uppermost lower mantle with a harzburgite-enriched composition. The 0.8% contour corresponds to the Samoa gap near the 660 within the Samoa plume (see Figure 1). The red square is a corner point where $\delta\mathrm{V}_{\mathrm{OUT}} = 0.8\%$ for the smallest values of $\delta\mathrm{V}_{\mathrm{IN}}$ and H. In (a), the dashed lines show the combinations of $\delta\mathrm{V}_{\mathrm{IN}}$ and H consistent with an elevation of the 660 due to the presence of a temperature $\Delta\mathrm{T}$, indicated with solid circles. The yellow and white lines correspond to assumed basalt fractions of $f = 0$ and $f = 0.2$, respectively. In (b), the dashed lines show the values of $\delta\mathrm{V}_{\mathrm{IN}}$ consistent with harzburgite enrichment below the 660 for $f = 0$, $f = 0.05$, $f = 0.10$, and $f = 0.15$.

Figure5.pdf

Figure 5. The expected values of δV_{OUT} in the Samoa gap for a model of the Samoa plume as a continuous thermochemical upwelling across the transition zone that has elevated the 660 and includes a 100-km thick zone below the 660 with a harzburgite-enriched (basalt-depleted) composition. δV_{OUT} is determined as a function of the temperature anomaly ΔT and for variable basalt fraction. in the uppermost lower mantle.

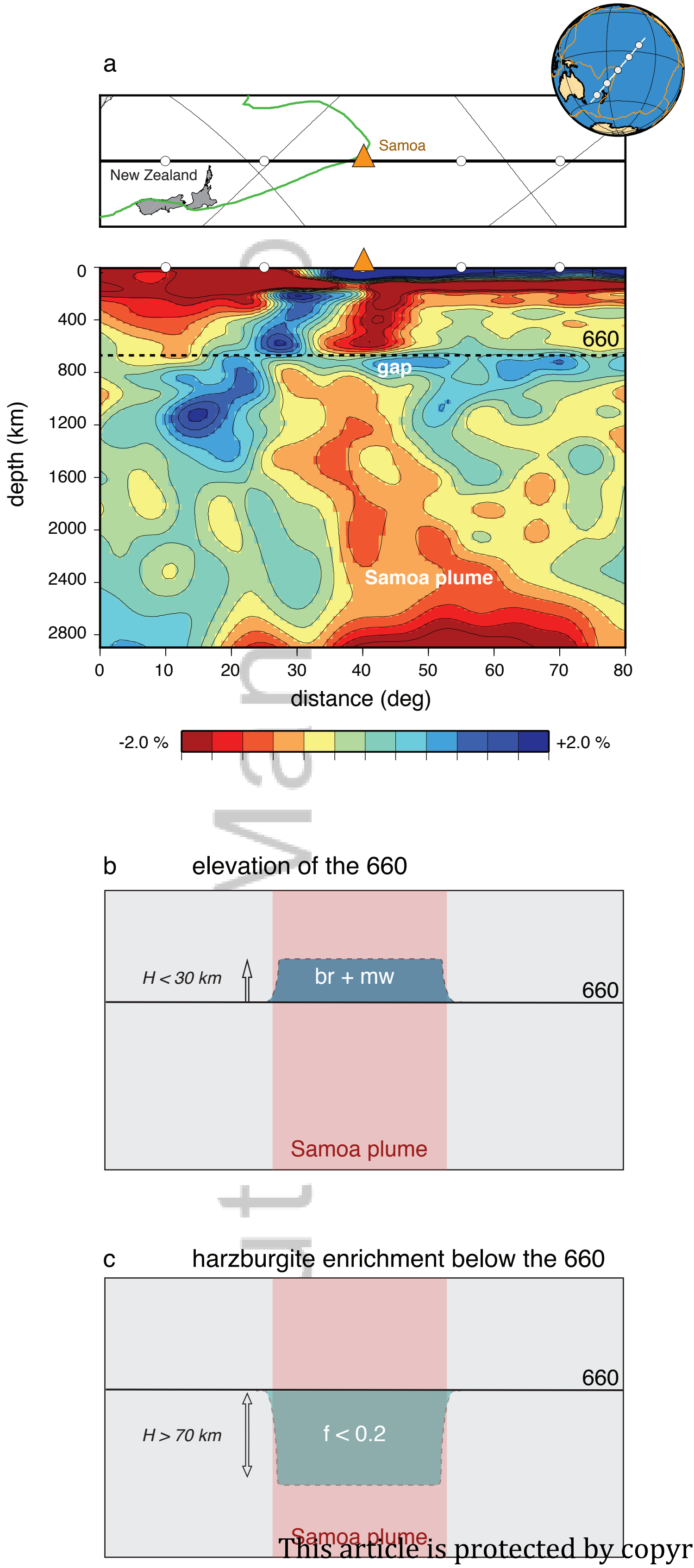
a
Samoa
New Zealand
depth (km)
0
400
800
1200
1600
2000
2400
2800
660
gap
Samoa plume
0
10
20
30
40
50
60
70
80
distance (deg)
-2.0 %
+2.0 %
b
elevation of the 660
H < 30 km
br + mw
660
Samoa plume
c
harzburgite enrichment below the 660
660
H > 70 km
f < 0.2
Samoa plume

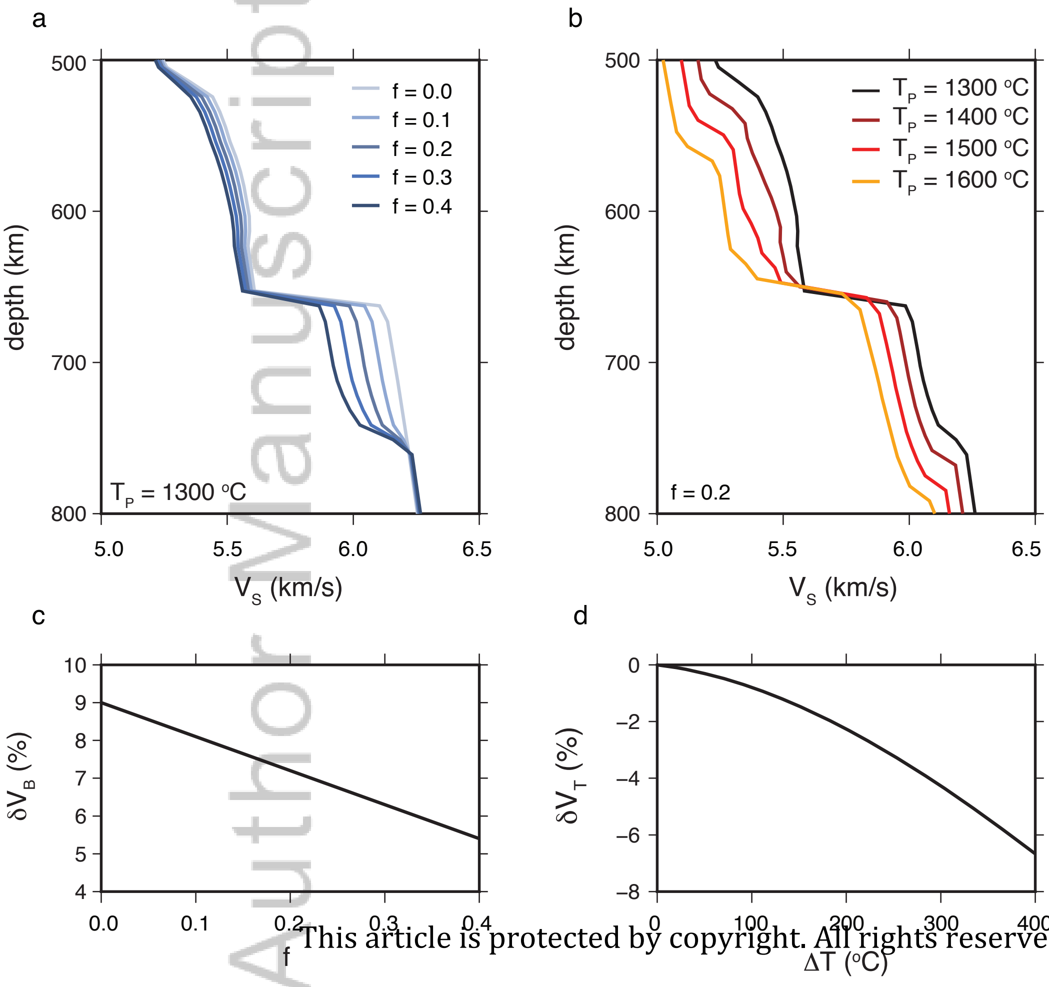
a
depth (km)
500
600
700
800
5.0
5.5
6.0
6.5
V_S (km/s)
f = 0.0
f = 0.1
f = 0.2
f = 0.3
f = 0.4
T_P = 1300 °C
b
T_P = 1300 °C
T_P = 1400 °C
T_P = 1500 °C
T_P = 1600 °C
f = 0.2
c
δV_B (%)
10
9
8
7
6
5
4
0.0
0.1
0.2
0.3
0.4
f
d
δV_T (%)
0
−2
−4
−6
−8
0
100
200
300
400
ΔT (°C)

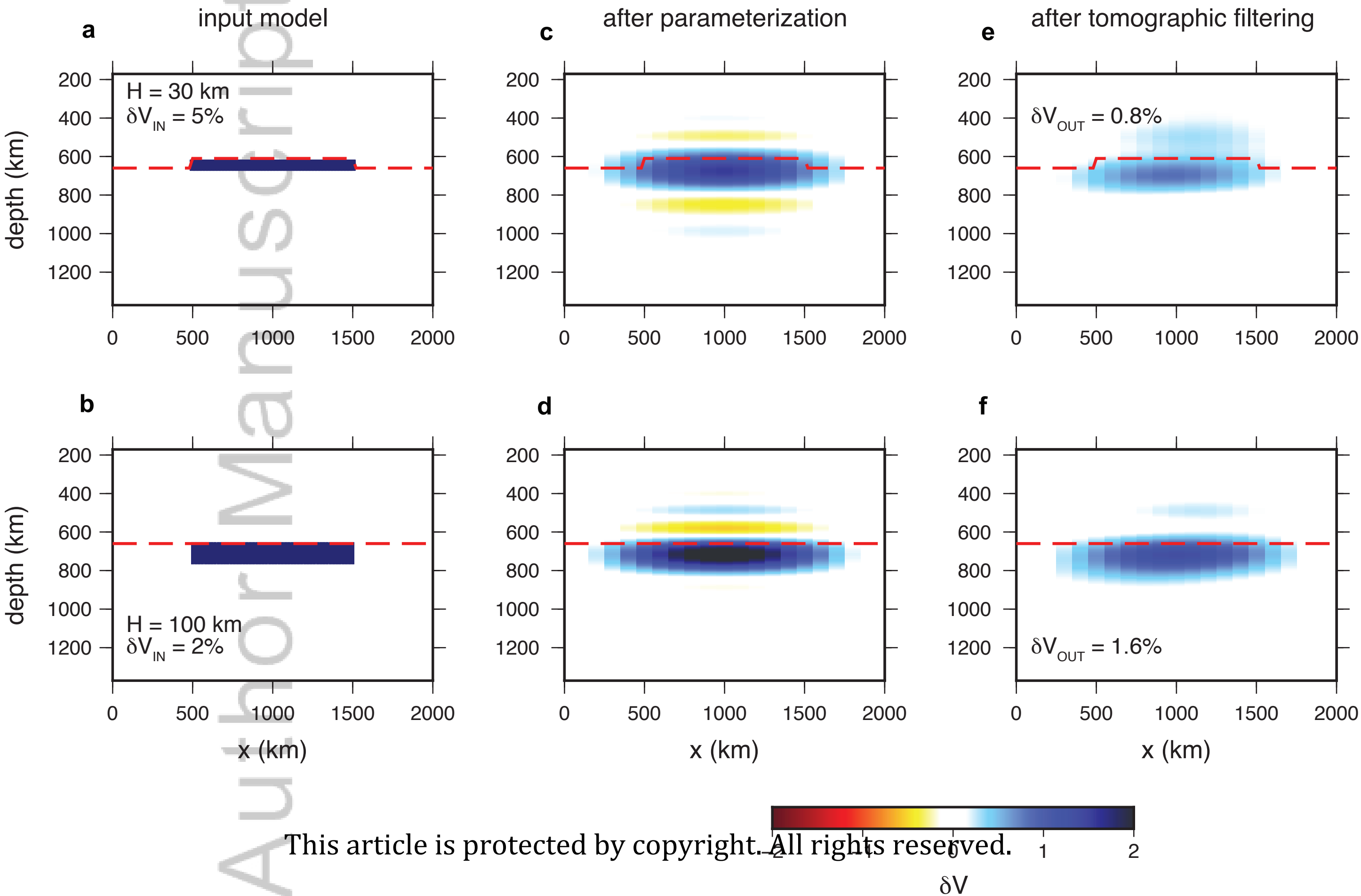

a
input model
H = 30 km
δV_IN = 5%
c
after parameterization
e
after tomographic filtering
δV_OUT = 0.8%
b
H = 100 km
δV_IN = 2%
d
f
δV_OUT = 1.6%
depth (km)
200
400
600
800
1000
1200
x (km)
0
500
1000
1500
2000
-2
-1
0
1
2
δV

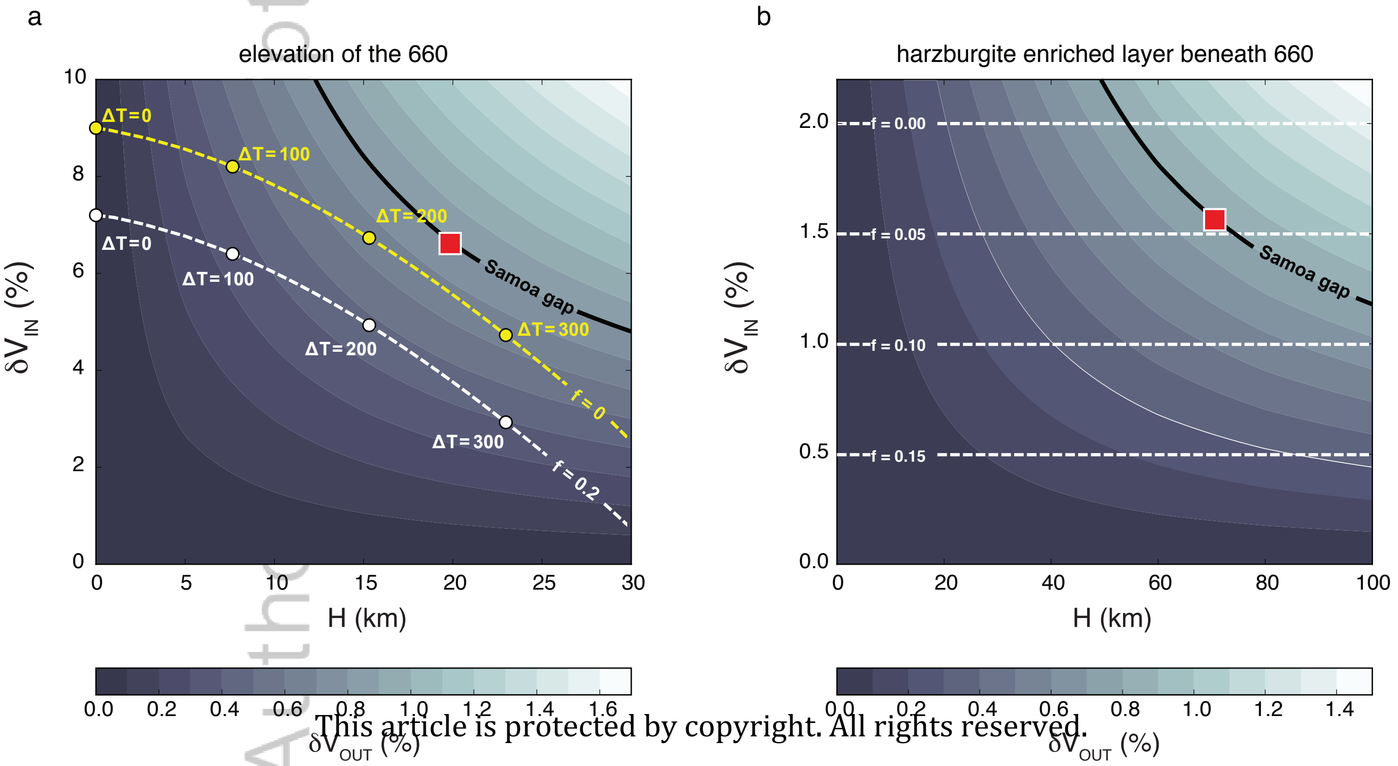
a
elevation of the 660
ΔT=0
ΔT=100
ΔT=200
ΔT=300
ΔT=0
ΔT=100
ΔT=200
ΔT=300
Samoa gap
f = 0
f = 0.2
δV_IN (%)
H (km)
δV_OUT (%)
b
harzburgite enriched layer beneath 660
f = 0.00
f = 0.05
f = 0.10
f = 0.15
Samoa gap
δV_IN (%)
H (km)
δV_OUT (%)

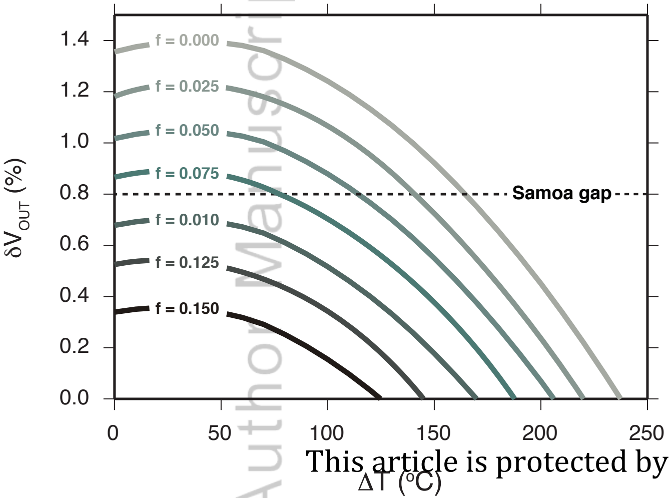

1.4
1.2
1.0
0.8
0.6
0.4
0.2
0.0
δV_OUT (%)
f = 0.000
f = 0.025
f = 0.050
f = 0.075
f = 0.010
f = 0.125
f = 0.150
Samoa gap
0
50
100
150
200
250
ΔT (ºC)